Acta Metallurgica Sinica (English Letters) (2022) 35:1935–1945
https://doi.org/10.1007/s40195-022-01428-0

Strengthening Mechanism and Microstructure of Deformable Ti Particles Reinforced AZ91 Composite

Biao Tang[1] · Jian-Bo Li[1,2] · Jun-Liu Ye[1] · Huan Luo[1] · Yi-Tao Wang[1] · Bo Guan[1] · Yang-Fan Lu[1] · Xian-Hua Chen[1] · Kai-Hong Zheng[3] · Fu-Sheng Pan[1]

Received: 17 March 2022 / Revised: 28 April 2022 / Accepted: 3 May 2022 / Published online: 23 June 2022

Abstract
In this study, the deformable titanium (Ti) particles reinforced AZ91 composite was successfully prepared by powder metallurgy and subsequent extrusion. The mechanical properties and microstructural evolution of pure AZ91 and 5Ti/AZ91 composite were studied. The yield strength, ultimate tensile strength, and elongation of 5Ti/AZ91 composite are measured to be 212 MPa, 323 MPa, and 10.1%, respectively. Microstructure analysis revealed that Ti particles are elongated along the extrusion direction, forming a discontinuous strip Ti particles, fine precipitated $Mg_{17}Al_{12}$ phase inhibits dynamic recrystallization (DRX) behavior through Zener pinning effect and hinders the growth of matrix grains, resulting in refiner grains of 5Ti/AZ91 composite. Heterogeneous deformed Ti particles and magnesium (Mg) matrix to generate additional heterogeneous deformation-induced (HDI) strengthening. Heterogeneous deformation-induced strengthening mainly contributed to the increment of yield strength for 5Ti/AZ91 composite.

Keywords Magnesium matrix composites · Ti particles · Recrystallization · Mechanical properties · Heterogeneous deformation

1 Introduction

While Mg alloys have drawn considerable attention as promising lightweight materials due to their low density, high specific strength, and high specific stiffness [1], their poor plasticity and low strength have limited potential application [2]. Meanwhile, magnesium matrix composites are known to co-host advantages of matrix and reinforcement, realizing the lightweight and good toughness of the material [3]. Extensive research on magnesium matrix composites has been conducted in a variety of research fields, including aerospace, automotive, and medical care. Typically, ceramic reinforcements, such as SiC, TC_4, Al_2O_3, BN, and Y_2O_3, have been intensively investigated in traditional magnesium matrix composites, leading to high strength and hardness natures [4]. However, the interface between ceramic particles and Mg matrix is highly incoherent. In addition, the hard and brittle characteristics of ceramic materials always result in substantial internal stress in the micro area. Thus, the ceramic reinforced magnesium matrix composites usually exhibit high strength but low ductility. For example, Wang et al. [5] found that SiC_p/Mg composite maintained an incoherent interface between SiC and Mg, resulting in a plasticity as low as 1.6%. Hassan et al. [6] prepared Al_2O_3/Mg composite with an ultimate tensile strength of ~ 250 MPa with poor plasticity of ~ 6.9%.

Compared with ceramic particles, metal particles, such as Ni, Cu, Fe, Nd, and Ti have higher plasticity and elastic modulus. However, the transition metals, such as Cu, Nd, Ni, and Fe, are rarely employed as reinforcement elements in magnesium matrix composites due to the formation of brittle intermetallic phases with Mg, reducing

Available online at http://link.springer.com/journal/40195.

✉ Jian-Bo Li
lijianbo1202@cqu.edu.cn

✉ Xian-Hua Chen
xhchen@cqu.edu.cn

[1] School of Materials Science and Engineering, Chongqing University, Chongqing 400044, China

[2] International Joint Laboratory for Light Alloys (MOE), School of Materials Science and Engineering, Chongqing University, Chongqing 400044, China

[3] Institute of New Materials, Guangdong Academy of Sciences, Guangzhou 510650, China

the corrosion resistance of Mg matrix [7–9]. Meanwhile, the transition metals, such as Ti, keep better wettability with the Mg matrix. Both Ti and Mg are immiscible under equilibrium conditions, avoiding the formation of brittle intermetallic phases at the Mg/Ti interface [10]. Moreover, Ti particles have the advantages of lower density, higher melting point, excellent mechanical strength, good ductility, and thus considered one of the ideal reinforcement elements for magnesium matrix composites [11].

Accordingly, Ti particles have attracted more attention to replace traditional hard ceramic reinforcement particles for magnesium matrix composites [12]. Rashad et al. [13] adopted the semi-powder metallurgy method to prepare Ti particles reinforced magnesium matrix composite, and its elastic modulus, yield strength, and ultimate tensile strength are 12.1 GPa, 147 MPa, and 212 MPa, respectively. Pérez et al. [14] prepared pure Ti reinforced magnesium matrix composite through powder metallurgy and hot extrusion, in which tensile strength and elongation are as high as 160 MPa and 8% at room temperature. Yu et al. [15] used powder metallurgy to prepare ultra-fine-grained Ti/AZ31 composite with a fracture toughness of 13%.

Powder metallurgy is a mature method for producing high-performance magnesium matrix composites which have been widely used in the past decades [16]. For magnesium matrix composites prepared by powder metallurgy routes after hot extrusion, the properties of magnesium matrix composites could be greatly improved. Ye et al. [17] found that the ultimate tensile strength and elastic modulus of 9Ti/AZ31 increased by 23 MPa and 3.2 GPa, respectively, compared to pure AZ31 alloy. Sankaranarayanan et al. [18] found that the extruded magnesium matrix composites were reinforced by Ti particles, and their ultimate tensile strength and plasticity were 226 MPa and 8.0%, respectively. Wang et al. [19] noted that the ultimate tensile strength of 5SiC_p/AZ91 increased from 151 to 273 MPa after extrusion due to the significant grain refinement by DRX. Extrusion can increase dislocation density in the matrix, thereby increasing the strength of matrix, which facilitates the transfer of larger payloads to reinforcement [20]. Studies on synergistic deformation of particles themselves with matrix and their effects on recrystallization have focused on ceramic particles [21]. Therefore, it is very interesting to study the recrystallization behavior, particle evolution, and HDI strengthening of Ti particles-reinforced magnesium matrix composite.

With the above discussion, here we studied the microstructure of magnesium matrix composite reinforced by Ti particles after hot extrusion and the mechanical properties. Deformation behaviors of Ti particles in the AZ91 matrix, the effect of Ti particles on recrystallization, and HDI strengthening induced by Ti particles are discussed.

2 Experimental

2.1 Fabrication of Composite

The pure AZ91 and 5Ti/AZ91 composite are prepared by powder metallurgy and subsequent extrusion as shown in Fig. 1. Both pure Ti powder and AZ91 alloy powder are commercial powders with a purity of 99.9%. In an argon atmosphere, pure Ti powder (< 36 μm) and AZ91 powder (< 75 μm) were mixed in a ball mill at a speed of 80 r/min for 150 min. The weight ratio of stainless steel balls and powder was 10:1. Then, the ball-milled powder was hot press sintering under the conditions of 15 MPa and 500 °C for 30 min. The shape of the sintered product is a cylindrical shape with 80 mm in diameter and 30 mm in height. The billets of pure AZ91 and 5Ti/AZ91 composite were homogenized at 420 °C for 24 h. The samples were kept in a furnace at 350 °C for 1 h, then extruded into a rod (16 mm in diameter) with an extrusion ratio of 25:1.

2.2 Microstructure Characterization

The Rigaku D/max 2500PC X-ray diffractometer was used to identify the constituent phase. Microstructure observation was conducted using a Zeiss metallographic microscope. Microstructure and crystal orientation analysis of samples were conducted using a JEOLJSM-7800F scanning electron microscope (SEM) equipped with electron backscatter diffraction (EBSD). The observed microstructures are located at the center of the specimen, parallel to the extrusion direction. To observe the grain boundaries of specimens, mechanical polishing is required, followed by etching with picric acid (5.5 g picric acid, 5 ml acetic acid, 90 ml ethanol, 10 ml distilled water). EBSD sample is prepared to perform mechanical polishing first and then use commercial magnesium alloy polishing solution for electrolytic polishing.

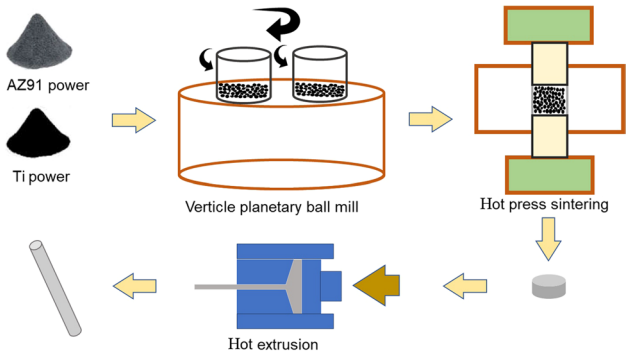

Fig. 1 Sketch map of fabrication procedure of Ti/AZ91 composite

2.3 Mechanical Properties

The tensile test of plate-shaped samples was conducted along the extrusion direction with a CMT-5105 universal testing machine at room temperature with a test rate of 1 mm/min. Tensile samples were tested three times under the same conditions to ensure reproducibility. The loading unloading–reloading (LUR) process of tensile test is carried out under a loading strain rate of 5×10^{-4} s^{-1}. Under a certain unloading strain, the specimen was unloaded in a load-control mode to 20 N at an unloading rate of 200 N min^{-1}, followed by reloading to the same applied load.

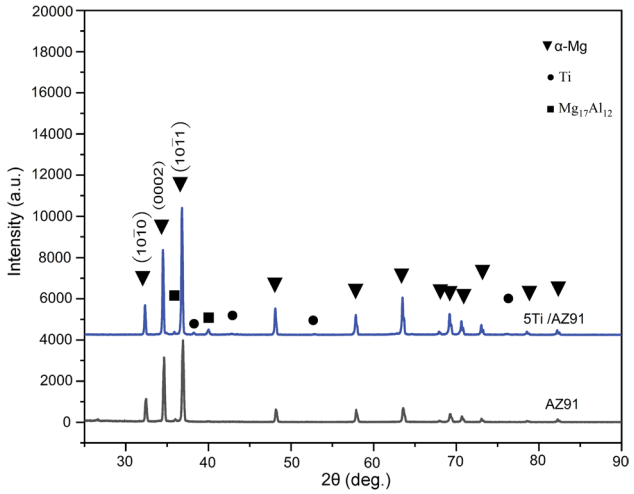

Fig. 2 XRD diagrams of as-extruded Ti/AZ91 composite

3 Results

The X-ray diffractometer (XRD) diffraction patterns of Ti/AZ91 composite are shown in Fig. 2. Diffraction peaks derived from the α-Mg matrix, Ti phase, and $Mg_{17}Al_{12}$ phase can be identified. The diffraction peaks at 32°, 34°, and 36° of diffraction pattern correspond to pyramid {10$\bar{1}$1}, basal {0002} and prismatic {10$\bar{1}$0} of magnesium alloy, respectively. No large amounts of other phases were found based on XRD results. It is well known that Mg and Ti will not dissolve with each other regardless of any temperature in an equilibrium state. Since XRD can only analyze phases with relatively large contents, the nanophases that may be precipitated require more microscopic characterization methods to confirm whether such compounds are formed at the interface.

Optical micrographs of Ti/AZ91 composite are shown in Fig. 3a and b. It can be seen that most of the grains in Fig. 3a are almost equiaxed, which indicates that DRX takes place after the extrusion. In 5Ti/AZ91 composite, it can be seen that Ti particles were elongated along the extrusion direction, forming a discontinuous strip Ti particles, as shown by the blue arrows in Fig. 3b.

After hot extrusion, the surface of Ti/AZ91 composite exhibits a void-free structure (Fig. 4). According to energy dispersive spectroscopy point scan results (Fig. 4c) and XRD analysis (Fig. 2), the fine second-phase particles in pure AZ91 alloy were identified as $Mg_{17}Al_{12}$. In the 5Ti/AZ91 composite, as shown in Fig. 4b, Ti particles appeared in the matrix, in addition to many fine $Mg_{17}Al_{12}$ dispersed. Ti particle distribution in the matrix was relatively uniform without agglomeration. As can be seen in Fig. 4d, the distribution map of 5Ti/AZ91 composite under high magnification, that

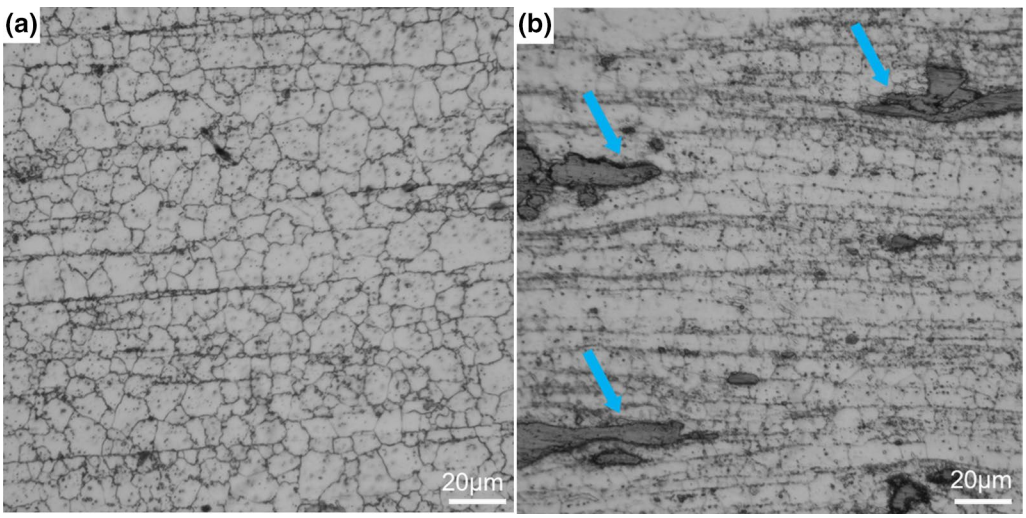

Fig. 3 Optical micrographs of as extruded **a** AZ91, **b** 5Ti/AZ91 composite

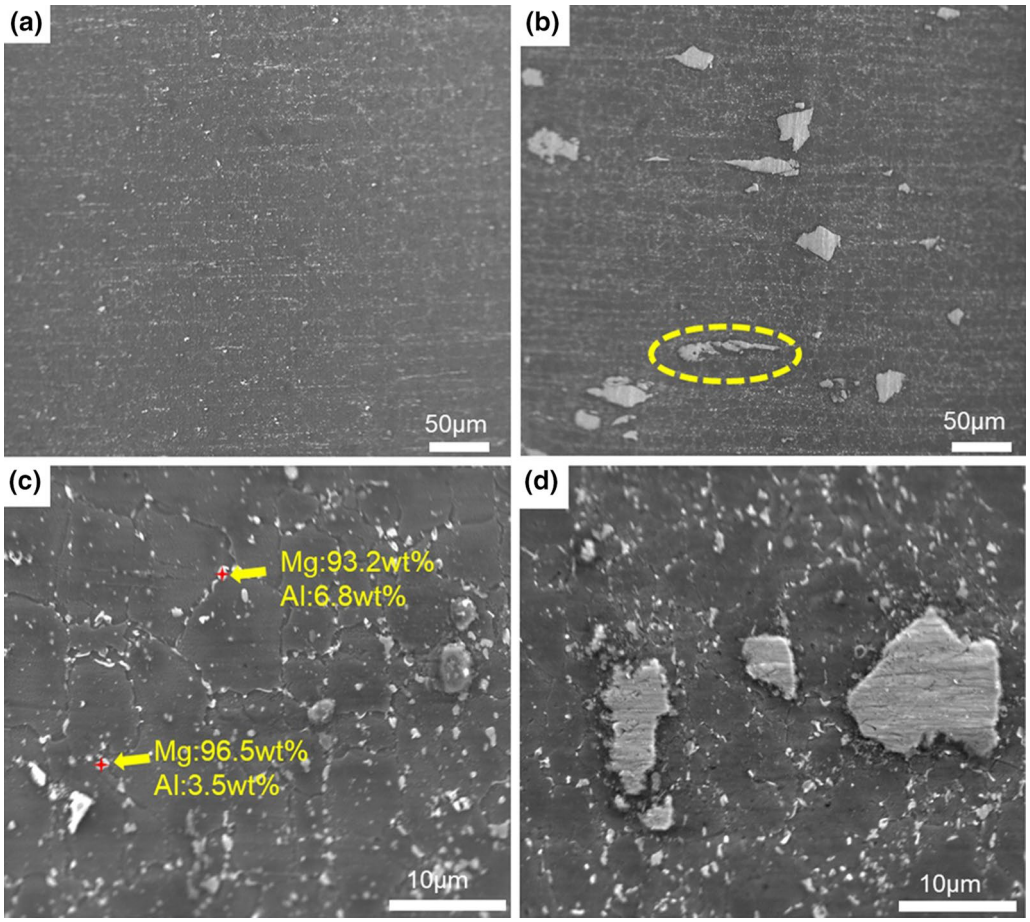

Fig. 4 SEM micrographs of as extruded **a, c** AZ91, **b, d** 5Ti/AZ91 composite

Ti particles are well combined with matrix interface without obvious voids.

The band contrast diagrams of Ti/AZ91 composite are shown in Fig. 5a and b. It can be seen that the grains of 5Ti/AZ91 composite are significantly smaller than those of pure AZ91, and the average grain sizes of AZ91 and 5Ti/AZ91 composite are 8.6 μm and 5.3 μm, respectively. There are bimodal structures in extruded 5Ti/AZ91 composite, which contain fine-equiaxed and coarse grains extending along the extrusion direction. Kernel average misorientation (KAM) diagrams of AZ91 and 5Ti/AZ91 composite are shown in Fig. 5c and d. It can be seen that local misorientation of crystal grains in pure AZ91 is lower than that in 5Ti/AZ91 composite. High KAM values indicate more stress concentration in the 5Ti/AZ91 composite. Recrystallization diagrams of AZ91 and Ti/AZ91 are shown in Fig. 5e and f. It can be seen from the figures that pure AZ91 alloy after extrusion, the volume fraction of recrystallized Mg matrix is as high as 87.4%. Meanwhile, the volume fraction of recrystallized Mg reduced to 59.1% in 5Ti/AZ91 composite. It is considered that there are more subgrain boundaries and strain energy in the structure, which can improve the strength of the material [22]. The recrystallization completion degree of 5Ti/AZ91 composite is lower than that of pure AZ91. In the matrix of 5Ti/AZ91, there are more deformed grains and substructures, which are more likely to form dislocation congestion groups, causing stress concentration. Under the action of external load, microcracks are more likely to occur in 5Ti/AZ91 composite. When stress is higher than the interface bonding strength, cracks will initiate and propagate rapidly during the subsequent deformation process, which is harmful to material's plasticity.

The tensile curves and mechanical properties values of Ti/AZ91 composite obtained by hot press sintering and subsequent hot extrusion are shown in Fig. 6a and b. It can be seen that the yield strength and ultimate tensile strength of 5Ti/AZ91 are as high as 212 MPa and 323 MPa, respectively. Compared to AZ91 alloy, the mechanical properties of the 5Ti/AZ91 composite are significantly improved. Table 1 summarizes yield strength, ultimate tensile strength, and elongation of magnesium matrix composites with different reinforcements. Compared to previous studies, the 5Ti/AZ91 composite has higher plasticity while improving strength, and its elongation is ~ 10%.

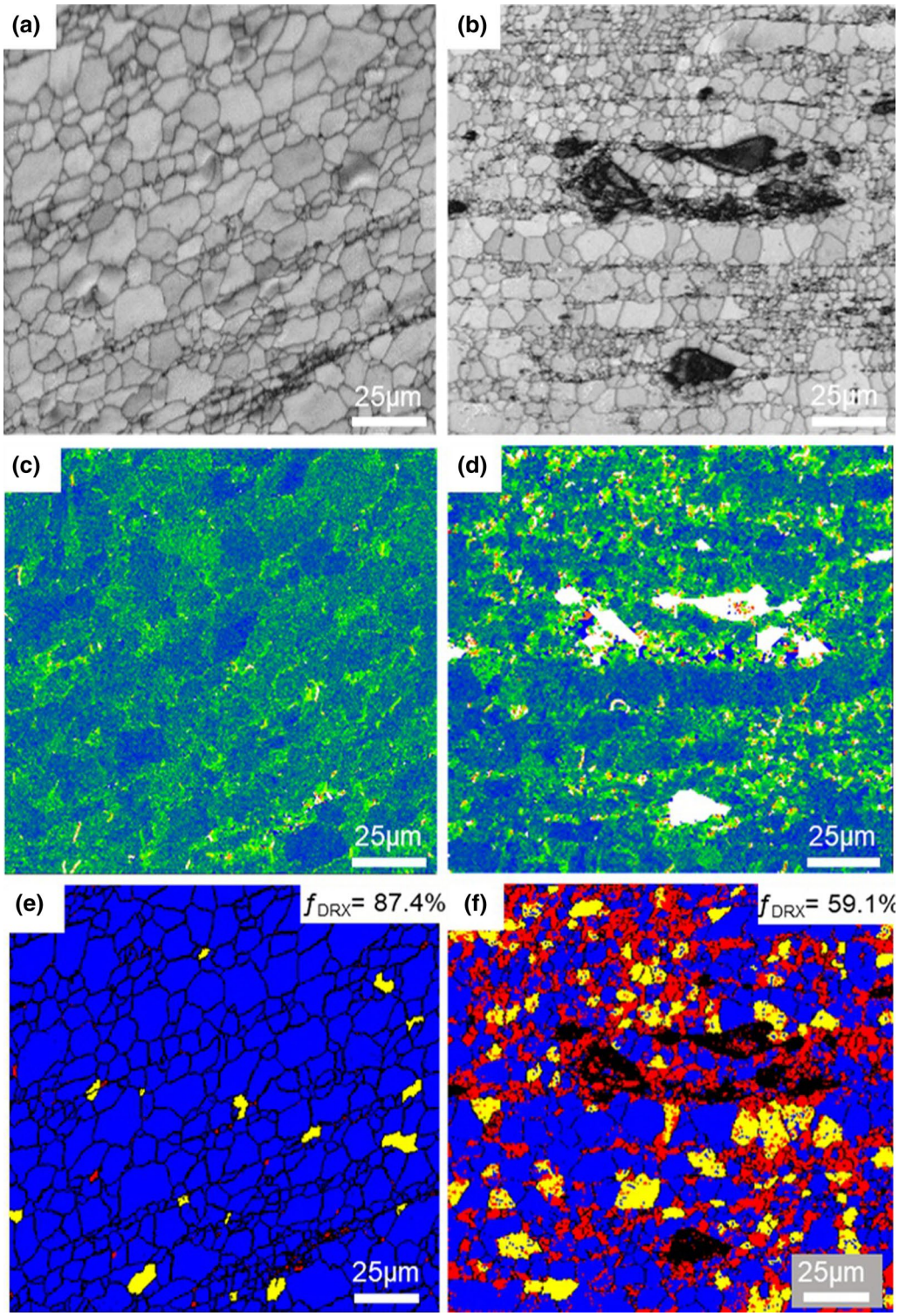

Fig. 5 Band contrast maps, KAM maps and DRX distribution maps of as extruded: **a**, **c**, **e** AZ91, **b**, **d**, **f** 5Ti/AZ91 composite

Tensile fracture morphologies of Ti/AZ91 composite are shown in Fig. 7. As marked by the yellow arrows in Fig. 7b, an amount of dimples can be identified in AZ91 material, indicating that the main fracture mechanism of AZ91 is ductile fracture, consistent with moderate elongation. In Ti/AZ91 composite, Ti particles are circled by the yellow ellipses, shown in Fig. 7c. Dimples and cleavage steps can be identified in the 5Ti/AZ91 composite.

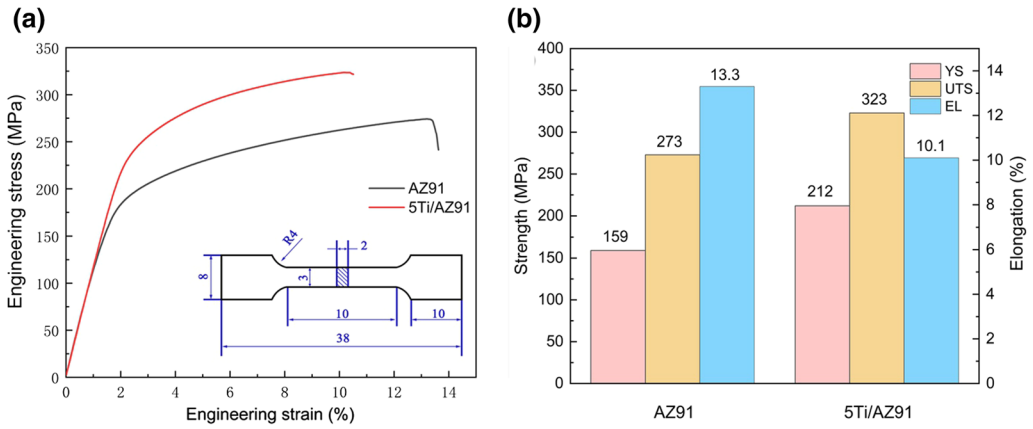

Fig. 6 **a** Tensile stress–strain curves, **b** tensile properties of as extruded AZ91 and 5Ti/AZ91 composite

Table 1 Mechanical properties of magnesium-based composite reinforced by different reinforcements

Composites	Processing method	Yield strength (MPa)	Ultimate tensile strength (MPa)	Elongation (%)	Ref.
5%Ti/AZ91	Hot press sintering + hot extrusion	212 ± 5	323 ± 5	10.1 ± 0.5	This work
10%Ti/Mg	Powder metallurgy + hot extrusion	118	158	1.5	[14]
3%Ti/Mg	Spark plasma sintering + Hot extrusion	192	251	8.9	[23]
20%Ti/Mg	Hot press sintering + hot extrusion	99	156	2.4	[24]
6%Ti/AZ31	Cold pressing + hot extrusion	255	304	6.9	[17]
5%Ti/AZ31	Vacuum hot pressing + hot extrusion	193	260	13.5	[15]

However, compared with the pure AZ91 alloy, the number of dimples and cleavage steps in the 5Ti/AZ91 composite is less than that of the pure AZ91 alloy. There are some cracks around Ti particles, as shown by the yellow arrows in Fig. 7d. Cracks around ceramic particles are more significant than those around Ti particles, and there are cracks through the matrix in the fracture diagram [25, 26]. After applying tensile load, cracks are more likely to initiate at the interfaces between ceramic particles and Mg. Since Ti and Mg have similar crystal structures, it is beneficial to achieve good interfacial bonding between Mg and Ti, which can delay propagation and connection of microcracks and prevent premature fracture of composite [27]. Mordike et al. [28] have reported that non-uniformity of deformation increases between particles and matrix in tensile tests, which leads to more stress concentrations around particles. During tensile deformation, a large stress concentration zone will appear around Ti particles, which is conducive to the initiation of microcracks at the Mg/Ti interface, resulting in a 3% decrease in ductility of the material.

4 Discussion

4.1 Stress–Strain Evolution of Particles

In the 5Ti/AZ91 composite, Ti particles are deformed into discontinuous strip Ti particles under the strong shear stress generated by extrusion. During extrusion, deformed Ti particles still maintain an excellent interface bond with the Mg matrix, as shown in Fig. 4b and d. There is a key issue in determining Ti particles' deformation during hot extrusion effectively. The force on the Ti particles must be greater than their yield strength, which would result in the plastic deformation of Ti particles. In principle, the best way to achieve this goal is to apply shear stress at the interface. The yield strength of Ti is about 218 MPa [29]. According to shear lag theory, only a small fraction of Ti particles can be loaded to yield stress. Moreover, the stress sustained by Ti particles is underestimated when using the shear lag theory. Because there is a difference in thermal expansion coefficient between Ti particles and

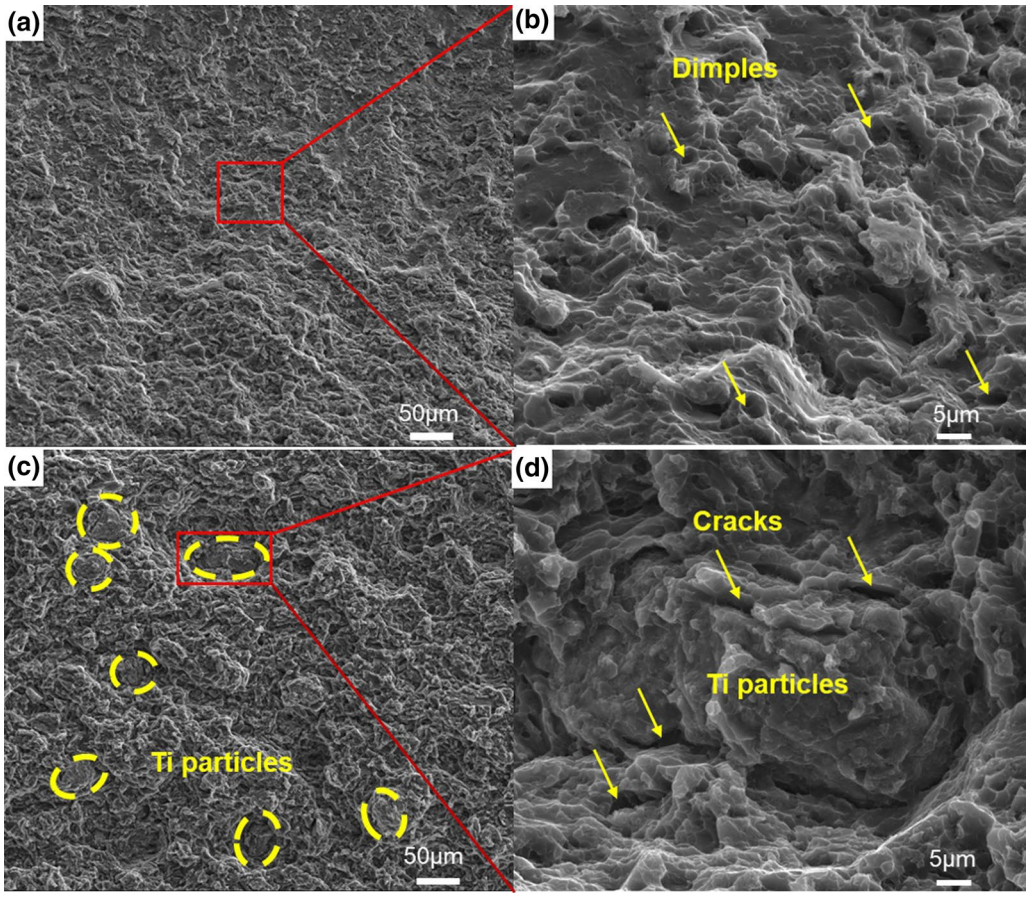

Fig. 7 Tensile fracture morphologies of as extruded **a**, **b** AZ91, **c**, **d** 5Ti/AZ91 composite

AZ91 matrix [30], the internal stress of composite is not taken into account. The residual stress (σ_{rp}) in the particles is given by [31]:

$$\sigma_{rp} = -\frac{2(1-V_p)E_m}{3(1-\vartheta_m)\varepsilon^*}, \tag{1}$$

where V_p is Ti particles volume fraction, ε^* is the Eigen strain, E is the modulus of AZ91, υ_m is Poisson's ratio of the matrix, which is given by the following equation [31]:

$$\varepsilon^* = -\frac{3m\Delta\alpha\Delta T_1}{(1-V_p)(m+2)} + 3mV_p, \tag{2}$$

$$m = \frac{(1-\vartheta_m)E_p}{(1-2\vartheta_m)E_m}, \tag{3}$$

In the above formula, $\Delta\alpha$ is the difference between the thermal expansion coefficients (CTEs) of two materials. E_m and E_p represent Young's modulus of matrix and particles, respectively. The parameter values used to calculate the residual stress are listed in Table 2. During solution treatment, ΔT_1 is the temperature change caused by quenching, which is 400 °C, and the above equation predicts the stress of Ti particles in 5Ti/AZ91 composite to be σ_{rp} = –396 MPa. The results show that Ti particles will be loaded to the yield strength during the hot extrusion process. As shown in Fig. 4 (b), Ti particles are elongated or even broken along the extrusion direction after extrusion marked by yellow dashed lines. It should be noted

Table 2 Parameter values for calculating residual stress and the increased yield strength [15, 17, 22, 30]

G (GPa)	b (nm)	ΔT (K)	$\Delta\alpha$ (°C^{-1})	V_p	d_p (μm)	σ_m (MPa)	υ_m	E_m (GPa)	E_p (GPa)
17.3	0.321	603	26.1×10^{-5}	0.02	25	159	0.33	45	106

that the equation assumed that particles have not undergone plastic deformation. However, considering the deformability of Ti particles, synergistic deformation behaviors of Ti particles may occur during tensile tests. Residual stress in the Ti particles is significantly released due to the plastic deformation of Ti particles.

4.2 Recrystallization Analysis

The main recrystallization mechanism of magnesium alloy at a relatively high temperature of 350 °C is discontinuous dynamic recrystallization (DDRX) deformation [32]. Incomplete recrystallization during hot deformation is considered the main reason for the existence of bimodal structures [33]. Large strain applied during extrusion causes grains to be elongated along the extrusion direction, and dislocation density gradually increases, leading to the occurrence of DDRX of Mg matrix. However, dislocations that are piled up around grain boundary can relieve local strain through strain-induced grain boundary migration, causing grain boundary bulging. As a result, boundary acts as a nucleation site for DRX grains formed by DDRX, and subsequent growth of newly formed grains (DRXed grains) reduces the internal strain energy of material [34]. Robson et al. [35] found that smaller second phase particles (size < 0.5 μm) can inhibit DRX behavior through Zener pinning effect. For larger particles (size > 1 μm), larger strain energy accumulates around the particles, which is beneficial to the formation of DRX grains around particles. This recrystallization phenomenon is called particle stimulated nucleation (PSN) [36].

It is well known that hard ceramic particles inhibit the flow of matrix during deformation, which gives rise to a local stress concentration around particles and thus reduces the plasticity of the material. Stress concentration at the interface between particles and matrix will produce a large number of high-density dislocations and large orientation gradients, thereby forming particle deformation zones (PDZs) [37]. However, Ti particles are elongated along the extrusion direction, which can release some of the stress concentration around particles. Therefore, under the same conditions, orientation gradient and dislocation density near Ti particles are lower than those of hard SiC particles. In 5Ti/AZ91composite, as a result of coordination deformation of Ti particles, the kinetic of Mg recrystallization weakened during hot extrusion. After hot extrusion, a larger density of defects (e.g. vacancies and dislocations) are generated, which provide more diffusion paths for solute elements and promote the formation of precipitates. Due to the uncoordinated deformation of Ti particles and Mg during extrusion, the density of crystal defects in 5Ti/AZ91 composite will be increased, which is conducive to the diffusion of aluminum, thereby promoting the precipitation of fine $Mg_{17}Al_{12}$ particles [33]. The distribution and size of $Mg_{17}Al_{12}$ in matrix significantly affect the degree of recrystallization of material [38]. As shown in Fig. 4d, there are more fine precipitates in 5Ti/AZ91 composite, which can delay DRX through Zener pinning effect. Fine $Mg_{17}Al_{12}$ reduces grain boundary mobility through the boundary pinning effect, so that boundary expansion required for nucleation of new DRX grains is suppressed, thereby reducing the DRX degree of material [39]. The volume fraction of recrystallized Mg in 5Ti/AZ91 composite is lower than the volume fraction of recrystallized Mg in pure AZ91 alloy due to the pinning effect generated by more $Mg_{17}Al_{12}$ in 5Ti/AZ91 composite. In terms of grain growth, fine $Mg_{17}Al_{12}$ precipitates inhibit the growth of DRXed grains, resulting in significant grain refinement of DRXed grains [36]. Statistical results of grain size in Fig. 5a and b show that the average grain size of 5Ti/AZ91 composite after extrusion is significantly smaller than the extruded pure AZ91 material.

4.3 Strengthening Mechanism

It is well known that the yield strength of composite is directly related to the ability of the material to delay the movement of dislocations. In AZ91 and Ti/AZ91 materials, Orowan strengthening, fine-grained strengthening, thermal mismatch strengthening, and load transfer strengthening contributed to the improvement in strength. In 5Ti/AZ91 composite, the Orowan strengthening effect is not significant, due to the coarser Ti particles and large inter particles spacing. The addition of Ti particles leads to grain refinement, which improves the yield strength of composite, according to the Hall–Petch relationship can be estimated [40]:

$$\Delta\sigma_{\text{Hall - petch}} = K\left(d_{\text{composite}}^{-\frac{1}{2}} - d_{AZ91}^{-\frac{1}{2}}\right), \tag{4}$$

where K is the Hall-Patch coefficient of Mg matrix which is given as 0.13 MPa·m$^{1/2}$. $d_{\text{composite}}$ and d_{AZ91} are the average grain size of composite and AZ91 alloy, respectively.

The difference in coefficient of thermal expansion between Ti particles and Mg matrix induces thermal strain, which generates a high density of dislocations near Ti particles, resulting in the improvement of yield strength of composite. The enhancement in yield strength can be calculated using the following equation [41]:

$$\Delta\sigma_{\text{CET}} = \sqrt{3}\alpha G b\sqrt{\frac{12V_{\text{p}}\Delta\alpha\Delta T}{(1-V_{\text{P}})bd_{\text{p}}}}, \tag{5}$$

where G is the shear modulus of AZ91 alloy, b is the Burgers vector of Mg, and α is the geometric constant value of 1.25. $\Delta\alpha$ is the CTEs different from the Ti particles and AZ91 matrix, ΔT represents the temperature difference between hot

extrusion temperature and tensile temperature. d_p and V_p are the average diameters and volume fraction of Ti particles, respectively.

In Ti/AZ91 composite, the load can be transferred from the Mg matrix to Ti particles, which is beneficial to improving the material's yield strength. The enhancement in yield strength caused by the load transfer ($\Delta\sigma_{load}$) can be calculated using the following equation [42]:

$$\Delta\sigma_{load} = 0.5V_p\sigma_m, \tag{6}$$

where σ_m is the yield strength of AZ91 matrix. The parameter values used to calculate the theoretical yield strength are shown in Table 2. Based on the above analysis, the theoretical yield strength ($\Delta\sigma$) of 5Ti/AZ91 composite can be calculated by the following equation:

$$\Delta\sigma = \Delta\sigma_{AZ91} + \Delta\sigma_{Hall-petch} + \Delta\sigma_{CET} + \Delta\sigma_{load}. \tag{7}$$

The theoretical yield strength of 5Ti/AZ91 composite is calculated and compared with the experimental results, as shown in Fig. 8. The values of $\Delta\sigma$ are lower than the experimental value. It can be seen that the four mechanisms are insufficient to explain the yield strength of AZ91 composite enhanced by heterogeneous Ti particles. Zhu et al. [43] believe that in steel, inhomogeneity caused by second phase or hard precipitates of different sizes will significantly increase the strength of the material. However, to achieve the goal that the strength and plasticity of material are increased simultaneously, heterogeneous domains with appropriate size, geometric shape, and distribution are required [44]. In this study, Ti particles were elongated along the extrusion direction to form discontinuous strip Ti particles, and Ti and Mg matrix still maintain a continuous interface. Plastic deformation between Ti particles and Mg matrix is inhomogeneous but continuous, resulting in strain gradient in domain interfaces, which needs to be accommodated by geometrically necessary dislocations (GNDs) [45]. The GNDs pile up at the domain interfaces produce back stress in the soft domain, resulting in HDI hardening that strengthens the soft domains [46]. However, the GNDs at the domain interface are hard to find alone. Meanwhile, HDI strengthening of particles-reinforced composite is still being explored. The HDI stress (σ_{HDI}) can be calculated by the following equation [47]:

$$\sigma_{HDI} = \frac{\sigma_u + \sigma_r}{2}. \tag{8}$$

In the above formula, σ_u unloading yield stress, and σ_r is the reload yield stress. The LUR test enables quantitative analysis of HDI hardening, as shown in Fig. 9a. The hysteresis loop of 5Ti/AZ91 composite during LUR test is larger, which means that the Bauschinger effect of 5Ti/AZ91 composite is stronger than that of pure AZ91 alloy, as shown in Fig. 9b. High magnification view of the hysteresis loops for determining the σ_u and σ_r is shown in Fig. 9c. Based on the calculation, the HDI stress of the 5Ti/AZ91 composite is much higher than the pure AZ91 alloy, as shown in Fig. 9d. The HDI stress of the 5Ti/AZ91 composite is about 21 MPa higher than the pure AZ91 alloy near the yield point. To trigger yielding in the 5Ti/AZ91 composite, additional external stress needs to be supplied [48]. In 5Ti/AZ91 composite, the GNDs pile up near Ti-Mg interfacial domain, which induces HDI strengthening and hardening, thereby the yield strength can be enhanced.

The calculated contribution of back stress to the yield strength of 5Ti/AZ91 composite is shown in Fig. 8. The calculated yield strength of 5Ti/AZ91 composite is 209 MPa, which is closed to the experimental value (212 MPa), compared with the AZ91 matrix, the increase in strength was mainly caused by HDI strengthening and thermal mismatch strengthening.

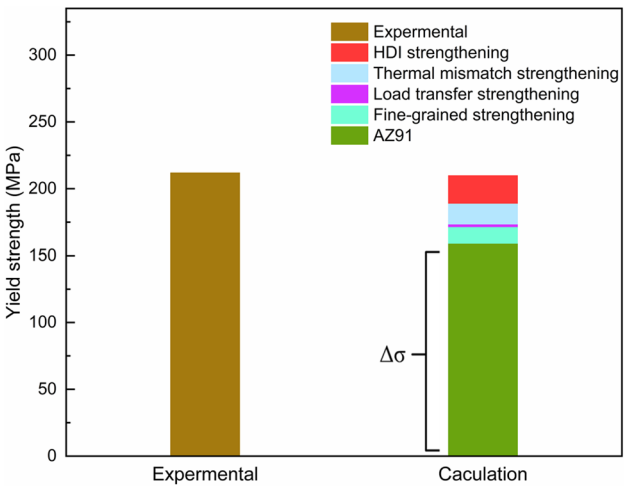

Fig. 8 Comparison between experimental and calculated YS of 5Ti/AZ91 composite

5 Conclusions

In this study, micron Ti particles are selected as the reinforcement, and the yield strength and fracture strength of the AZ91 alloy are increased greatly. Microstructure evolution, strengthening mechanism, and mechanical properties of Ti/AZ91 composite were studied. The main conclusions can be drawn as follows:

1. Ti particles can be deformed plastically during extrusion. Discontinuous strip Ti particles reinforced AZ91 composite can be formed after extrusion.

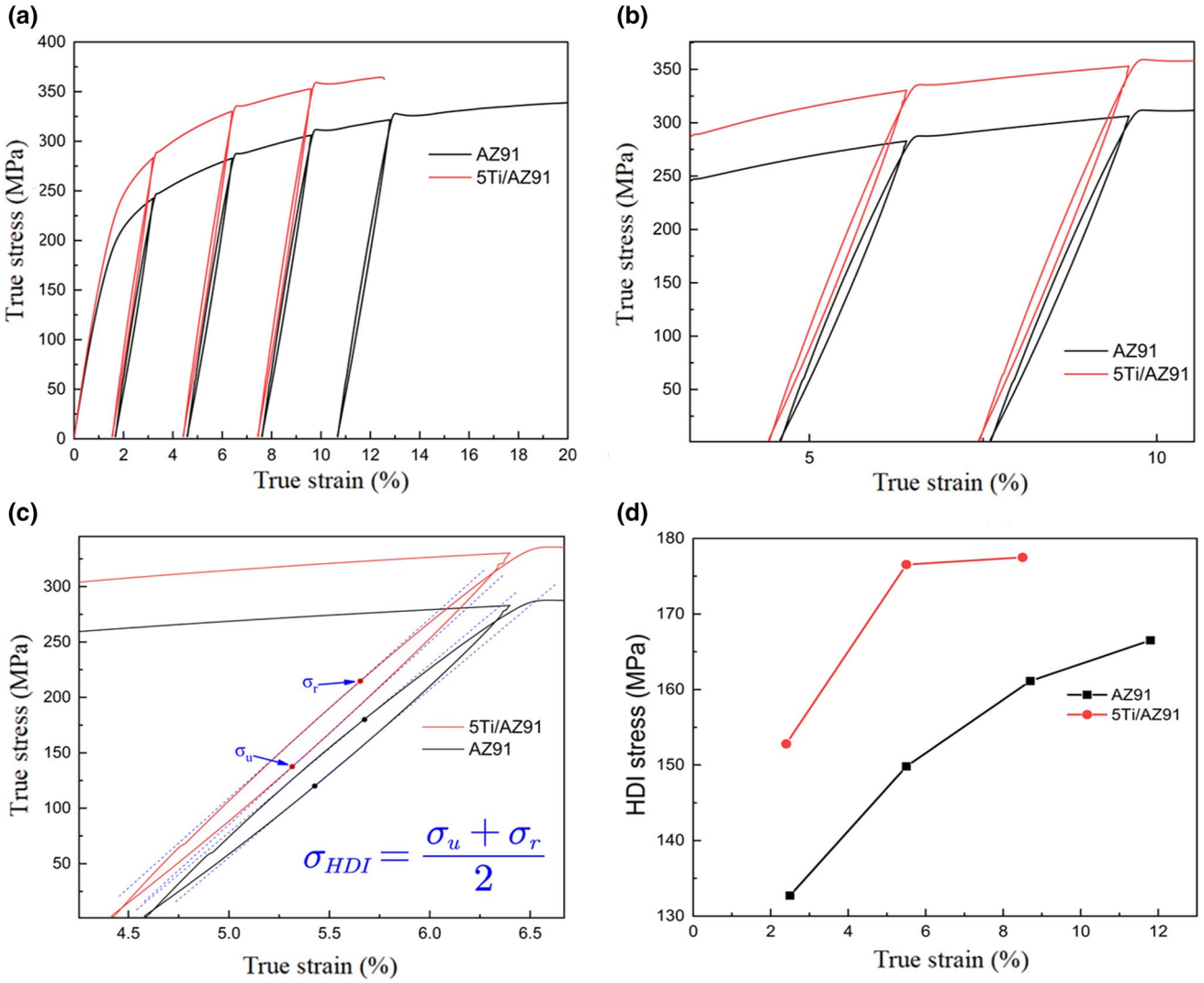

Fig. 9 HDI stress of Ti/AZ91 composite: **a** loading unloading–reloading stress–strain curves; **b** 2nd and 3rd cycles of hysteresis loop in high magnification view; **c** the 2nd measured hysteresis loop with σ_u and σ_r defined; **d** HDI stress of the two samples

2. The fine precipitated $Mg_{17}Al_{12}$ phase inhibits DRX behavior through Zener pinning effect. The Ti particles can promote the precipitation of $Mg_{17}Al_{12}$, and the recrystallization completion degree of 5Ti/AZ91 composite was reduced with the addition of Ti particles.
3. The yield strength and ultimate tensile strength of 5Ti/AZ91 composite are 212 MPa and 323 MPa, respectively. Heterogeneous deformation-induced strengthening mainly contributed to the increment of yield strength for 5Ti/AZ91 composite.

Acknowledgements This word was financially supported by the Guangdong Major Project of Basic and Applied Basic Research (No. 2020B0301030006), the National Natural Science Foundation of China (Nos. 52171133 and 52171103), the "111 Project" (B16007) by the Ministry of Education and Fundamental Research Fund of Central Universities in China (No. 2018CDJDCL0019).

Declaration

Conflict of interest The authors state that there are no conflicts of interest to disclose.

References

[1] L. Liu, X. Chen, F. Pan, J. Magnes. Alloy. **9**, 1906 (2021)
[2] J. Hu, Q. Li, H. Gao, Acta Metall. Sin. -Engl. Lett. **34**, 65 (2021)
[3] F. Ning, Q. Le, Y. Jia, L. Chen, Acta Metall. Sin. -Engl. Lett. **34**, 1255 (2021)
[4] C. Ding, X. Hu, H. Shi, W. Gan, K. Wu, X. Wang, J. Magnes. Alloy. **9**, 1363 (2021)

[5] X. Wang, N. Wang, L. Wang, X. Hu, K. Wu, Y. Wang, Y. Huang, Mater. Des. **57**, 638 (2014)
[6] S. Hassan, M. Gupta, Mater. Sci. Eng. A **392**, 163 (2005)
[7] Z. Yu, X. Xu, B. Du, K. Shi, K. Liu, S. Li, X. Han, T. Xiao, W. Du, Acta Metall. Sin. -Engl. Lett. **1**, 13 (2021)
[8] W. Wang, P. Han, P. Peng, T. Zhang, Q. Liu, S. Yuan, L. Huang, H. Yu, K. Qiao, K. Wang, Acta Metall. Sin. -Engl. Lett. **33**, 43 (2020)
[9] Q. Li, X. Peng, F. Pan, J. Magnes. Alloy. **9**, 2223 (2021)
[10] Q. Li, Q. Luo, Y. Chen, J. Wang, B. Jiang, F. Pan, Int. J. Miner. Metall. Mater. **29**, 32 (2022)
[11] B. Wang, D. Xu, S. Wang, L. Sheng, R. Zeng, E. Han, Int. J. Fatigue **120**, 46 (2019)
[12] Q. Li, Y. Lu, Q. Luo, X. Yang, Y. Yang, J. Tan, Z. Dong, J. Dang, J. Li, Y. Chen, B. Jiang, S. Sun, F. Pan, J. Magnes. Alloy. **9**, 1922 (2021)
[13] M. Rashad, F. Pan, M. Asif, J. She, A. Ullah, J. Magnes. Alloy. **3**, 1 (2015)
[14] P. Pérez, G. Garcés, P. Adeva, Compos. Sci. Technol. **64**, 145 (2004)
[15] H. Yu, H. Zhou, Y. Sun, L. Ren, Z. Wan, L. Hu, Adv. Powder Technol. **29**, 3241 (2018)
[16] S. Jayasathyakawin, M. Ravichandran, N. Baskar, C. Anand, R. Balasundaram, Mater. Today **27**, 736 (2020)
[17] J. Ye, J. Li, H. Luo, J. Tan, X. Chen, B. Feng, K. Zheng, F. Pan, Mater. Sci. Eng. A **833**, 142526 (2022)
[18] S. Sankaranarayanan, R. Sabat, S. Jayalakshmi, S. Suwas, M. Gupta, J. Alloy. Compd. **575**, 207 (2013)
[19] X. Wang, X. Hu, K. Nie, K. Wu, M. Zheng, Trans. Nonferrous Met. Soc. China **22**, 1912 (2012)
[20] M. Godzierz, M. Olszowka, N. Sobczak, R. Nowak, P. Wrzesniowski, J. Magnes. Alloy. **9**, 156 (2021)
[21] A. Jiang, Z. You, Z. Duan, G. Qiao, J. Zhang, L. Guo, China Foundry **18**, 565 (2021)
[22] M. Hu, S. Wei, Q. Shi, Z. Ji, H. Xu, Y. Wang, J. Magnes. Alloy. **8**, 841 (2020)
[23] J. Umeda, M. Kawakami, K. Kondoh, E. Ayman, H. Imai, Mater. Chem. Phys **123**, 649 (2010)
[24] X. Cai, S. Ding, Z. Li, X. Zhang, K. Wen, L. Xu, Y. Zhang, T. Shen, Compos. B Eng. **215**, 108743 (2021)
[25] K. Deng, C. Wang, K. Nie, X. Wang, Acta Metall. Sin. -Engl. Lett. **32**, 413 (2019)
[26] X. Luo, H. Liu, L. Kang, J. Lin, D. Zhang, D. Li, D. Chen, Acta Metall. Sin. -Engl. Lett. **35**, 757 (2021)
[27] P. Li, B. Cao, W. Tan, M. Gao, J. Alloy. Compd. **818**, 152925 (2020)
[28] B. Mordike, P. Lukáč, Surf. Interfaces **31**, 682 (2001)
[29] D. Li, G. Fan, X. Huang, D. Juul Jensen, K. Miao, C. Xu, L. Geng, Y. Zhang, T. Yu, Acta Mater. **206**, 116627 (2021)
[30] M. Hassan, J. Alloy. Compd. **345**, 246 (2002)
[31] D. Monaghan, Comput. Mater. Sci **9**, 99 (1997)
[32] T. Jonas, Acta Metall. **32**, 1637 (1984)
[33] Y. Li, M. Zha, H. Jia, S. Wang, H. Zhang, X. Ma, T. Tian, P. Ma, H. Wang, J. Magnes. Alloy. **9**, 1556 (2021)
[34] X. Wang, X. Hu, K. Nie, K. Deng, K. Wu, M. Zheng, Mater. Sci. Eng. A **545**, 38 (2012)
[35] J. Robson, D. Henry, B. Davis, Acta Mater. **57**, 2739 (2009)
[36] J. Go, J. Lee, H. Yu, S. Park, J. Mater. Sci. Technol. **44**, 62 (2020)
[37] Z. Zhu, K. Nie, P. Munroe, K. Deng, Y. Guo, J. Han, Mater. Chem. Phys. **259**, 124048 (2021)
[38] L. Doherty, F. Humphreys, J. Jonas, D. Jensen, M. Kassner, W. King, T. McNelley, H. McQueen, A. Rollett, Mater. Sci. Eng. A **238**, 219 (1997)
[39] T. Zhao, Y. Hu, B. He, C. Zhang, T. Zheng, F. Pan, Mater. Sci. Eng. A **765**, 138292 (2019)
[40] L. Liu, X. Zhou, S. Yu, J. Zhang, X. Lu, X. Shu, Z. Su, J. Magnes. Alloy. **10**, 501 (2020)
[41] N. Chelliah, H. Singh, R. Raj, M. Surappa, Mater. Sci. Eng. A **685**, 429 (2017)
[42] L. Chen, J. Xu, H. Choi, M. Pozuelo, X. Ma, S. Bhowmick, J. Yang, S. Mathaudhu, X. Li, Nature **528**, 539 (2015)
[43] Y. Zhu, K. Ameyama, P. Anderson, I. Beyerlein, H. Gao, H. Kim, E. Lavernia, S. Mathaudhu, H. Mughrabi, R. Ritchie, N. Tsuji, X. Zhang, X. Wu, Mater. Res. Lett. **9**, 1 (2020)
[44] H. Wu, G. Fan, Prog. Mater. Sci **113**, 100675 (2020)
[45] J. Liu, K. Zhao, M. Zhang, Y. Wang, L. An, Mater. Lett. **143**, 287 (2015)
[46] X. Wu, M. Yang, F. Yuan, G. Wu, Y. Wei, X. Huang, Y. Zhu, Proc. Natl. Acad. Sci. U. S. A. **112**, 14501 (2015)
[47] Z. Li, X. Fang, Y. Wang, P. Jiang, J. Wang, C. Liu, X. Wu, Y. Zhu, C. Koch, Mater. Sci. Eng. A **777**, 139074 (2020)
[48] M. Yang, Y. Pan, F. Yuan, Y. Zhu, X. Wu, Mater. Res. Lett. **4**, 145 (2016)